Using Metal-Organic Frameworks for the Catalytic Dehydrogenation of Ammonia Borane

Sanjay Kumar Keshava
Mentor: Dr. Suresh Babu Kalidindi

Materials Science Department
PPISR
July 2019

Contents

List of Figures

Executive Summary

With the excessive use of fossil fuels resulting in global warming and climate change, there is an ever increasing need to find alternative sources of energy that are clean and renewable. Hydrogen presents itself as an attractive option as water is the only by-product of its combustion. This is where the concept of a hydrogen economy enters the picture. If hydrogen that is produced renewably is used as an on-board fuel in vehicles, it would help combat global warming and climate change. The main problem with the on-board use of hydrogen is its storage. Due to its extremely low density, it is very challenging to store hydrogen on-board without compromising on the cost, safety, efficiency, sustainability or practicality of the system. A possible solution to this problem involves the use of solid-state hydrogen storage materials. Here, a novel compound known as ammonia borane (AB) presents itself as a viable option as it has significant advantages over conventional solid-state hydrogen storage materials (such as metal-hydrides) that make it more favourable. AB can be dehydrogenated in a non-aqueous solvent to release hydrogen and form products which can be used to regenerate AB, but it is plagued by sluggish kinetics. The aim of this study was to engineer highly effective catalysts for the dehydrogenation of AB in the non-aqueous medium. Due to their tunable nature, ultrahigh porosity, large internal surface areas, and overall physical and chemical properties, metal-organic frameworks (MOFs) emerge as possible candidates for high-performance catalysts. This study looks at the photocatalytic activity of cerium based MOFs with the UiO-66 architecture for AB dehydrogenation. Using light to control the rate of AB dehydrogenation is convenient, as it does not require high temperatures on-board. Cerium based MOFs with the UiO-66 architecture were chosen due to their photocatalytic properties and overall chemical and physical stability. The investigation also looks at the possible synergistic effects of embedding platinum nanoparticles within the MOFs, and introducing amine groups on the photocatalytic activity of the MOFs. We studied 4 catalysts (UiO-66 cerium MOF, Pt@UiO-66 cerium MOF, NH_2UiO-66 cerium MOF and Pt@NH_2-UiO-66 cerium MOF) and we found that all of them exhibited photocatalytic activity. Unfortunately, none of the catalysts were effective enough so as to be useful in on-board hydrogen storage systems. Nevertheless, this study has opened up numerous possibilities that could involve tuning the properties of the cerium based MOFs to make them efficient photocatalysts for AB dehydrogenation in hydrogen storage systems.

Chapter 1

Introduction

1.1 Fossil Fuels and Global Warming

To accommodate for the needs of a growing population, and allow for rapid industrial and agricultural development, large quantities of fossil fuels are being used as a source of energy [1]. When burned, these non-renewable fuels release carbon dioxide (CO_2), a greenhouse gas, into the atmosphere. Greenhouse gases trap infrared radiation which is emitted from the Earth's surface and prevent it from escaping into space. Although this helps maintain temperatures which are necessary for the sustenance of life on Earth, in recent years, the overuse of fossil fuels has led to rapidly increasing atmospheric CO_2 levels which is enhancing the greenhouse effect and causing an unfavourable rise in average global temperature [2].

Before the industrial age, CO_2 levels in the atmosphere averaged at around 280 ppm (parts per million), but they have risen to almost 410 ppm today [3]. On average, the global surface temperature has risen by approximately 1.0 °C since the year 1880 [4]. An increase of 1.0 °C may seem insignificant, but given the large heat capacity of the Earth and its oceans, it takes a truly substantial amount of heat energy to raise the average yearly surface temperature by even a tiny amount. Scientists predict that if CO_2 levels cross the 550 ppm value, and the average yearly surface temperature of the planet rises by a further 1.0 °C, it could lead to irreversible location dependent climate change. Extreme precipitation events resulting in heavy rainfall maybe noticed in some regions of the world, while others may experience recurring heat waves and lasting droughts. Furthermore, increasing global temperatures could encourage the thermal expansion of ocean water, and the melting of polar ice caps, thus causing sea levels to rise. This could increase the risk of low-lying lands being flooded [5, 6]. In fact, we are already seeing examples of these changes all around the world. In the coming years, conditions may become so harsh as to threaten the existence of all life on Earth [7]. Apart from the problem of global warming, there is also the question of being able to meet the world's energy demands. The demand

for energy will only rise due to the increasing population, and the urbanization that is taking place. Fossil fuels can only act as a temporary solution because they are non-renewable fuels. It is estimated that, the world's fossil fuel reserves will be completely depleted in 40 years for petroleum, 60 years for natural gas, and 156 years for coal. For all these reasons, there is an urgent need to find alternative sources of energy which are both clean and renewable.

Worldwide efforts are being made to drastically reduce CO_2 emissions and there is an ongoing search for sources of energy that can replace fossil fuels. Here, hydrogen presents itself as a viable alternative, especially as an on-board fuel for vehicles, and this is where the concept of a hydrogen economy comes into the picture [8]. There are numerous advantages associated with the use of hydrogen as a primary fuel. Since the combustion of hydrogen produces water as the only product, it is immediately an attractive option as a clean source of energy. Using hydrogen as a fuel may help reduce CO_2 emissions significantly, thus slowing the onset of global warming and climate change. That apart, in comparison to fossil-fuels, hydrogen has a much higher gravimetric energy density (energy per unit mass). While most fossil fuels and hydrocarbon fuels have a gravimetric energy densities between 20-55 MJ/kg, hydrogen's is nearly 120 MJ/kg [9]. In essence, hydrogen is a very light fuel [10]. In comparison to fossil fuels, hydrogen is a far more environmentally friendly option, and if produced by sustainable methods, it is a renewable source of energy. Clearly, the use of hydrogen as a fuel has its benefits. But it comes with its own challenges. If we truly wish to switch to a hydrogen based economy, much research work needs to be undertaken in the areas of hydrogen production, storage and use.

Although hydrogen is the most abundant element in the universe, it does not occur in nature in its molecular form (H_2). It is most often found in chemical compounds, like hydrocarbons or water. Therefore, to produce hydrogen, these compounds must be chemically modified. As of today, the majority of world's hydrogen is produced from natural gas by steam reforming. Coal gasification is also a popular, cost-effective option. But with both these methods, the whole point of using hydrogen is lost, because the production of hydrogen now uses non-renewable fossil fuels and releases CO_2 into the atmosphere. There is much research being done on finding new methods of hydrogen production which are both clean and renewable [8, 11, 12, 13]. One promising option is to use renewable sources of energy such as solar, wind, hydro, or geothermal energy to produce electricity. This electrical energy can then be used to electrolyse water, thus producing hydrogen in a clean and renewable fashion. As an alternative to electrolysis, there is the possibility of solar powered thermochemical water splitting which can be used to generate hydrogen from water. Metal oxide semiconductor materials with the ability to split water via photocatalysis (by absorbing visible light) are also another attractive option. Furthermore, multiple biological methods are also being looked into. Researchers are trying to replicate manganese-oxygen clusters which have been used for billions of years by plants to split water at room temperature. There is also work being done on the production of hydrogen by biomass processing. In conclusion, although the majority of the worlds hydrogen is currently produced from non-renewable fossil

fuels while emitting CO_2 into the atmosphere, scientists are making significant progress in finding new ways to produce hydrogen in a clean and renewable manner. In the coming years, it is likely that most of the worlds hydrogen will be produced by these methods, thus paving the way for a world where hydrogen is the primary fuel.

The storage of hydrogen is the next big hurdle. In particular, the on-board storage of hydrogen as a fuel for use in vehicles is a big challenge. For suitable on-board storage, a high volumetric energy density (energy per unit volume) is essential because of the limited volume available for the fuel tank in vehicles. A low volumetric energy density means that the vehicle will be unable to travel for long distances without being re-fuelled multiple times, and in the case of hydrogen this is in fact one of the main issues making its use impractical. Even though hydrogen has a high gravimetric energy density, due its extremely low density, it ends up with a low volumetric energy density (even if stored under pressure). To better illustrate the problem, an approximate calculation to compare hydrogen and gasoline is presented below. Let $\mathrm{D_g}$ and $\mathrm{D_h}$ be the densities of gasoline and hydrogen respectively (at room temperature and pressure). Similarly, let $\mathrm{G_g}$ and $\mathrm{G_h}$ be their gravimetric energy densities, and let $\mathrm{V_g}$ and $\mathrm{V_h}$ be their volumetric energy densities. Then, we notice that,

$$D \times G = V$$

We can now use some approximate values for $\mathrm{D_g}$, $\mathrm{D_h}$, $\mathrm{G_g}$, and $\mathrm{G_h}$ to calculate the values of $\mathrm{V_g}$, $\mathrm{V_h}$ and the ratio $\mathrm{V_g/V_h}$ to help us effectively compare gasoline and hydrogen as on-board fuels (at room temperature and pressure) [9, 14].

$$D_{\mathrm{g}} \approx 740 kg/m^3 \quad \text{and} \quad G_{\mathrm{g}} \approx 45 MJ/kg$$

$$\implies V_{\mathrm{g}} \approx 33300 MJ/m^3$$

Similarly, we get that,

$$D_{\mathrm{h}} \approx 0.089 kg/m^3 \quad \text{and} \quad G_{\mathrm{h}} \approx 120 MJ/kg$$

$$\implies V_{\mathrm{h}} \approx 10.7 MJ/m^3$$

Therfore, we get that,

$$V_{\mathrm{g}}/V_{\mathrm{h}} \approx 3120$$

The efficiency of a gasoline powered internal combustion engine, $\mathrm{E_g}$ is roughly 20% while that of a hydrogen powered fuel cell, $\mathrm{E_h}$ is around 60% [8]. We can factor this into our ratio by multiplying it by $\mathrm{E_g/E_h}$. Our new ratio, $\mathrm{Q_g/Q_h}$ gives us the ratio of the distances a vehicle with a full tank can theoretically travel when it is gasoline powered versus when it is hydrogen powered. This

assumes room temperature and pressure. It also assumes that all the other variables such as the volume of the fuel tank, the speed of vehicle during motion, the mass of the vehicle, etc. are the came in both cases. Therfore, we obtain

$$Q_{\mathrm{g}}/Q_{\mathrm{h}} \approx 3120 \times (0.20/0.60) \approx 1040$$

This clearly illustrates the problem at hand. A gasoline powered vehicle with a full tank can travel roughly 1000 times further than a hydrogen powered vehicle with a full tank. It is clear that to ensure that $Q_{\mathrm{g}}/Q_{\mathrm{h}} \approx 1$ we will need to increase the density of hydrogen substantially. This means that the pressure under which hydrogen must be stored has to be increased by a large amount. It is possible to store hydrogen under high pressure in gas cylinders, but it is very costly, and also highly dangerous due the flammable nature of hydrogen. Furthermore, the storage containers are very heavy, bulky and take up a lot of space. The alternative option of storing hydrogen as a cryogenic liquid at low temperatures means that about 40 percent of its energy is lost in the process of liquefaction. Also, like storage at high pressures, it is faced with same problems. Although these methods of storage are the most commonly used, they are not suitable for on-board storage purposes due to limited space, the involved risks, the energy loss and the associated costs. Because of this, there is much research being done on solid-state materials which can store hydrogen more efficiently [9]. Ultra-porous materials with high surface areas (such as metal-organic frameworks) are seen as possible candidates for hydrogen storage due to their hydrogen adsorption properties. But, often, in these materials, the adsorption is rather weak, and this means that the materials can only store hydrogen at very low temperatures. This is once again an issue. There is also work being done on materials which store hydrogen in the form of chemical bonds, here, metal hydrides present themselves as the most popular option. From many viewpoints, metal hydrides are very good hydrogen storage materials, but they have kinetic limitations. Since hydrogen is stored in the form of chemical bonds, it is not easy to release the hydrogen from the metal hydrides without heating them to high temperatures [15]. Hydrogen storage compounds such as magnesium nitrogen hydride and sodium borohydride have a high hydrogen content, but face the same problem as metal hydrides, thus making them unsuitable for on-board storage. Ideal solid-state hydrogen storage materials should be stable, have a high hydrogen storage capacity, and be able to release hydrogen under on-board ($0-100$ °C and $1-10$ atmospheres) conditions rapidly without requiring excessive energy input. From the sustainability perspective, reversibility is another important requirement. Ideally, after hydrogen hydrogen has been released, it should be possible to recombine the leftover products of the reaction with hydrogen to re-synthesize the material. Hydrogen storage is an area where much work remains to be done, and it is the biggest roadblock in the way of the hydrogen economy.

The final aspect of a hydrogen economy is the efficient use of hydrogen. Here, hydrogen fuel cells appear as suitable options for both on-board and off-board applications. The most popular fuel cells are the PEM (proton exchange

membrane) fuel cells [16]. Compared to hydrogen storage, research in the area of hydrogen usage has had much better progress. PEM fuel cells currently have an efficiency of about 60 percent while internal combustion engines based on gasoline have an efficiency of only around 20 percent. Furthermore, fuel cells are compact instruments with low operating temperatures and high durability (upto 7 years) which can use hydrogen and oxygen to produce electricity efficiently. The major issue with PEM fuel cells is their high cost. This is because platinum is used as a catalyst in PEM fuel cells. But as PEM fuel cells are being used more and more widely, the cost is projected to decrease over the years. Therefore, we should expect PEM fuel cell technology to become very affordable in the near future.

In conclusion, although there have been significant advances in the areas of hydrogen production and use, the storage of hydrogen is still a big problem. Much effort has been put into finding lightweight, solid state materials which can store a large quantity of hydrogen, and from which hydrogen can be released under mild temperatures at reasonable rates so as to be useful for on-board storage purposes. Here, a monomeric compound known as ammonia borane (NH_3BH_3) has attracted a lot of attention as it seems to possess many of these required properties.

1.2 Ammonia Borane and Hydrogen Storage

Ammonia borane (NH_3BH_3), often reffered to as AB, is a crystalline solid (at room temperature and pressure) that was successfully synthesised for the first time in 1955 [17]. Due to its physical and chemical properties, it is considered as a promising material for hydrogen storage purposes [18, 19, 20]. On-board hydrogen storage materials must meet a few important requirements which are as follows: 1) the storage material must be such that its volumetric energy density is high, as this ensures that frequent stops for refuelling are not necessary; 2) It must be possible for the material to release hydrogen at a reasonable rate, under the mild on-board conditions, even when the concentration of the material is low; 3) the material must produce as few volatile by-products as possible when hydrogen is released, as these can hamper the function of the PEM fuel cell; 4) the reaction by-products must be such that they can be recycled to regenerate the original material thus meeting the sustainability criteria; 5) large scale synthesis of the material must be possible in a cost-effective manner.

AB is a light compound with a density of roughly $0.78 g/cm^3$ and 19.6% of its weight is made up of hydrogen. Essentially, this means that AB has a high volumetric energy density as a small volume of AB stores many moles of hydrogen. As visible from its chemical formulas, if dehydrogenated completely, 1 mole of AB has the potential to release 3 moles of hydrogen. AB is stable in air at room temperature and pressure, thus making it easy to store and transport. AB is also stable when dissolved in water or weakly basic solvents, and in general, it tends to dissolve quite easily in most polar solvents. AB is analogous to ethane (CH_3CH_3), but it has very different chemical and physical

properties. AB has both hydridic hydrogen atoms (from the B-H bond) and protic hydrogen atoms (from the N-H bonds) which polarise the molecule and give it its chemical and physical properties. AB also has a very strong B-N bond which ensures that, under most conditions, the loss of hydrogen occurs rather than the dissociation into ammonia and borane. This is one of the primary reasons for our interest in AB.

There are multiple methods to synthesize AB, but the most popular one is salt metathesis [21]. This usually involves a reaction between an ammonium salt (such as ammonium sulphate or ammonium chloride) and sodium borohydride in an organic solvent. This is a fairly cost-effective method of AB synthesis with a high yield and purity, and although it is currently used only for laboratory synthesis, it is very likely that it will soon be used to produce AB on an industrial scale.

There is much research which is studying methods to effectively dehydrogenate AB, as this is a key aspect in being able to use it for on-board hydrogen storage purposes [22]. As of now, there are three basic methods by which AB can be dehydrogenated and they are as follows: 1) thermal dehydrogenation; 2) catalytic dehydrogenation in the aqueous medium; 3) catalytic dehydrogenation in the non-aqueous medium. Since 1 mole of AB can potentially release 3 moles of hydrogen, this is the ultimate target. According to thermodynamic analysis, the release of hydrogen from AB and its partially dehydrogenated products is favourable from both an enthalpy and an entropy perspective. This suggests that the regeneration of AB by using the reaction products via hydrogenation will require a large input of energy, thus making it impractical. However, the products of the reaction depend on the method by which AB was originally dehydrogenated. When AB is dehydrogenated, B-H bonds are broken, and the resulting products are composed mainly of B-O or B-N bonds. This changes the situation because different reaction products have different chemical properties, and so, they can be hydrogenated to regenerate AB with different levels of ease. Since the possibility of regeneration is important in terms of sustainability, we must consider all the cases carefully while keeping in mind the other requirements for on-board storage in order to find an optimal solution.

The thermal dehydrogenation of AB occurs in a series of steps and multiple products are formed [23, 24]. Overall, the chemistry looks similar to that of ethane dehydrogenation which produces ethene and ethyne. AB begins to release hydrogen when heated above room temperature and the first mole equivalent of H_2 is released at around 95 °C, this leaves behind aminoborane (analogous to ethene). AB melts at around 112 °C. The second mole equivalent of H_2 is released at around 150 °C, leaving behind iminoborane (analogous to ethyne). The last mole equivalent is of H_2 is released only at temperatures above 450 °C, and this leaves behind the highly stable boron nitride. Aminoborane and iminoborane are highly reactive, and they tend to form their addition polymers which are polyaminoborane and polyiminoborane respectively. Once again, this is much like how ethene and ethyne form their addition polymers, which are polyethene and polyethyne respectively. Small traces of borazine (analogous to benzene) also form during the reaction. Thermal dehydrogenation seems like

a simple and efficient method to extract the hydrogen from AB, but there are many drawbacks. The main issue is the extremely long induction time. This means that even at high temperatures, the hydrogen is released very slowly over many hours. The other issue is that, it is not possible to raise temperatures above 100 °C on-board just by using the heat generated from the fuel cell. This essentially means that only 1 mole equivalent of H_2 can be extracted from AB via thermal dehydrogenation on-board. Increasing the temperature to extract more hydrogen becomes an inefficient process and it is also difficult to do this under the mild conditions on-board. For these reasons, thermal dehydrogenation as a method to extract H_2 from AB on-board is not a practical one.

AB can be dehydrogenated in the aqueous medium using lewis acids or transition metals as catalysts [25]. For example, if a small amount of aqueous hydrochloric acid is added to a solution of AB in water, effervescence will be observed as hydrogen is released. If instead of aqueous hydrochloric acid, nanoparticles of a transition metal such as nickel are added, then the observed result is the same. In both the cases, 3 full mole equivalents of hydrogen are released extremely rapidly. The reaction often ends rather quickly, but of course, this depends on multiple factors such as the concentration of AB, the catalyst used, and the reaction temperature. It is well-known that the nanoparticles of platinum and rhodium in particular, although expensive, are highly active catalysts for the dehydrogenation of AB in the aqueous medium. This method of extracting hydrogen from AB is highly efficient, fast, and does not require high temperatures. In fact, the dehydrogenation often takes place quite fast even at room temperature, therefore, this is a feasible way to generate hydrogen on-board from AB. However, the majority of the products of this reaction are derivates of boric acid, and it takes extremely large amounts of energy to convert them back to AB due to unfavourable thermodyanamics. This is a major drawback to the aqueous chemistry involving AB as it does not meet the required goal of sustainability.

AB can also be dehydrogenated in the non-aqueous medium [23]. Here, transition metals are routinely used as catalysts just like in the aqueous medium. AB is usually dissolved in solvents such as diglyme or dioxane, and nanoparticles of a transition metal are added to release hydrogen. Unlike in the aqueous case, both the kinetics and the reaction products are entirely different in the non-aqueous case. The reaction products include cyclodiborazane, cyclotriborazane, borazine and the polymer polyborazylene. Like in the aqueous case, platinum and rhodium are good catalysts. However, comparatively, the kinetics are extremely slow and even with the best catalysts, hydrogen is evolved quite slowly. Furthermore, only around 1.5 mole equivalents of hydrogen are released. The positive aspect is that there is much work being done on using the reaction products to regenerate AB efficiently and some methods have already been reported. There is also work being done on finding highly efficient catalysts for the dehydrogenation of AB in the non-aqueous medium. Here, a unique class of porous nano-materials known as metal-organic frameworks attract much attention. Due to their tunable nature, it is possible to engineer metal-organic frameworks so that they can behave as efficient catalysts.

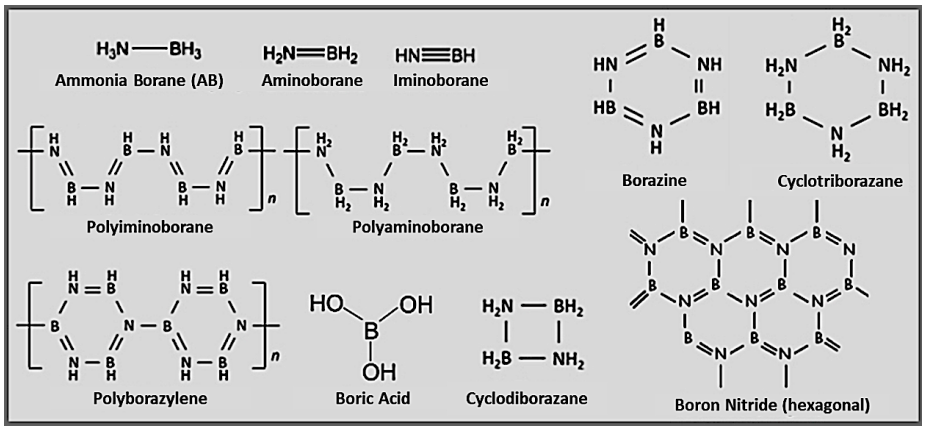

Figure 1.1: Derivatives of AB. Image adapted from references [18, 19, 26, 27].

1.3 Metal-Organic Frameworks and Catalysis

Metal-organic frameworks (MOFs) are an extensive class of crystalline coordination polymers that consist of both inorganic and organic components. The inorganic components are compact clusters called secondary building units (SBUs) and they consist of metal ions bonded strongly to ligands. The organic components are ligands (these are often bidentate or polydentate ligands). We can compare a MOF to a crystal of NaCl where every ion is surrounded by 6 ions of the opposite charge that are placed octahedrally [28]. In a typical MOF, SBUs are linked to each other by organic ligands in a regular, geometric pattern that extends into 1, 2 or 3 dimensions [29]. Another nice way to picture MOFs is to think of them as being polymers with coordination complexes as their repeat units. We can consider the UiO-66 cerium MOF as an example as it is the main MOF in this project. During the synthesis of this MOF, a cerium salt (ceric ammonium nitrate, $(NH_4)_2Ce(NO_3)_6$) and an organic ligand (terephthalic acid (H_2BDC) are mixed in solution. As the salt dissolves, Ce^{4+} ions enter the solution and combine with the ligand molecules to form $[Ce_6O_4(OH)_4]^{12+}$ clusters which are the SBUs. The SBUs now get linked to each other by the ligand molecules in a regular fashion, and this results in the formation of the MOF [30, 31]. The diagrams below show the structures of the ligand, the SBU and the MOF.

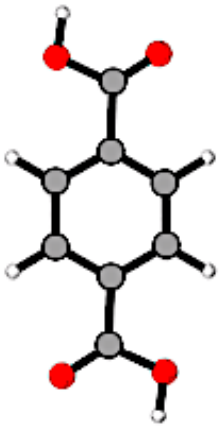

Figure 1.2: Terephthalic acid, the organic ligand. Atoms are colored as follows: C, gray; O, red; H, white. Image adapted from reference [32].

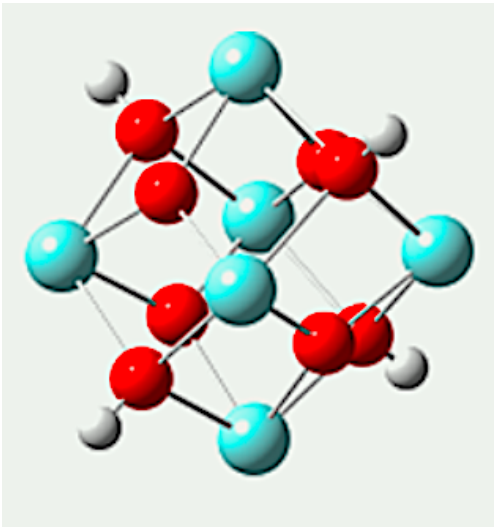

Figure 1.3: $[Ce_6O_4(OH)_4]^{12+}$, the SBU of the MOF. Atoms are colored as follows: O, red; H, white; Ce, light blue. Image adapted from reference [32].

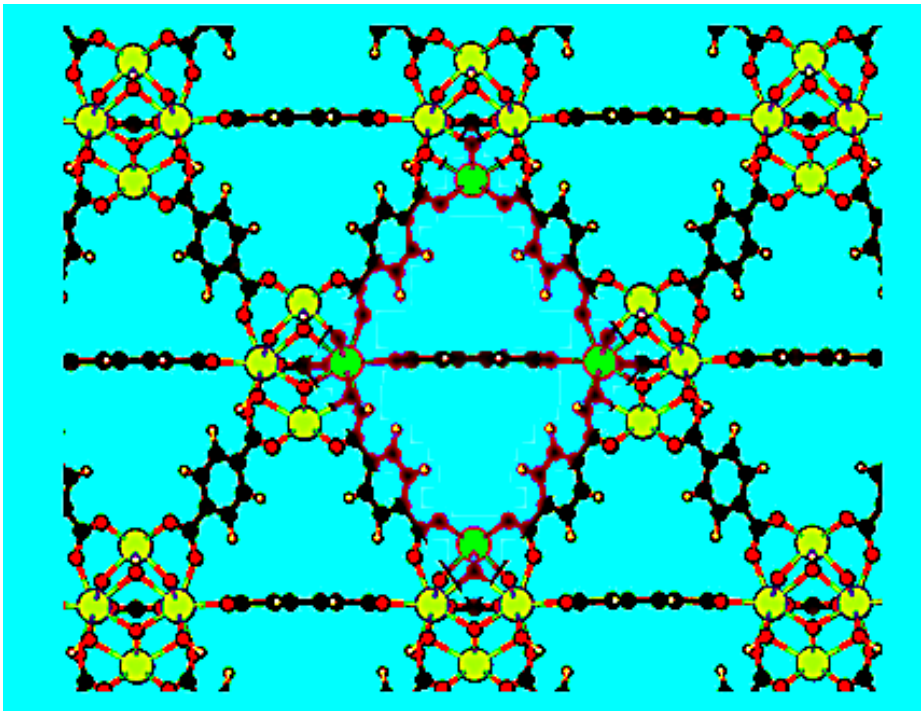

Figure 1.4: Structure of the UiO-66 cerium MOF. Atoms are colored as follows: C, black; O, red; H, white; Ce, yellow. Image adapted from reference [33].

There are numerous ways in which MOFs can be synthesised [34]. Solvothermal synthesis which involves mixing a metal salt with an organic ligand in a high boiling point solvent is the most commonly used method. The mixture is usually kept in an air tight container at a specific temperature for anywhere between 12 and 48 hours. Parameters such as the solvent, reagent concentration, pH, nature of the precursors used, temperature and time are varied according to the specific requirements. Some MOFs are difficult to synthesise directly. In such case, methods such as post-synthetic modification (PSM), solvent assisted linker exchange (SALE), and solvent assisted ion exchange (SAIE) are used to obtain the desired MOF. SALE and SAIE are used to replace organic ligands or metal ions respectively in the MOF without altering its underlying and architecture. PSM can be used to embed active sites (such as metal nanoparticles (MNPs)) into the pores of MOFs, support active sites on the surface of MOFs, and modify the organic ligands chemically to add new functional groups. MOFs can be used to create hybrid materials by embedding MNPs into their pores to create MNPs@MOF materials. MNPs can also be supported on the surface of MOFs to create hybrid MNPs/MOF materials. To synthesize MNPs@MOF materials, the standard ship-in-a-bottle approach which allows the MOF to grow

around pre-formed nanoparticles can be used [35]. Alternatively, the MOF can be mixed thoroughly with the solution of the metal precursor. This ensures that metal ions from the precursor enter the pores of the MOF. Then, they can reduced to form nanoparticles that remain trapped within the pores. MNPs/MOF materials are usually prepared by thoroughly mixing MOFs with pre-formed nanoparticles. After synthesis, MOFs need to be activated. The first step in the most common activation method involves washing the MOF (using a centrifuge) multiple times in the solvent used for synthesis to remove excess reactants and impurities. Next, a solvent exchange is performed by washing the MOF with a low boiling point solvent multiple times. This ensures that all of the original solvent is removed. Now, the MOF is dried under vacuum to remove the solvent and complete the activation. The solvent exchange process is done because evaporating high boiling point solvents from the pores of MOFs can damage their architecture.

Once MOFs have been synthesised and activated, they must be characterised to verify their crystal structure [34]. Basic MOF characterization involves powder X-ray diffractometry (PXRD). This involves plotting a diffraction pattern that can be used to analyse the crystal structure of the MOF. This can then be compared with standards to confirm that the particular MOF has formed successfully. Brunauer−Emmett−Teller (BET) analysis involves measuring the amount of gas that can be adsorbed within the MOF. This can be used to calculate the internal surface area and pore volume of the MOF. Inductively coupled plasma optical emission spectroscopy (ICP-OES) can be used to find the quantity of a given element in the MOF. This is often used to measure the quantity of MNPs that have embedded in MNPs@MOF materials or supported on MNPs/MOF materials. Bright field TEM (transmission electron microscopy) can be used to check if metal NPs are embedded within MOFs or supported on their surface. Fourier transform infrared spectroscopy (FTIR) can be used to detect specific functional groups and quantify them. X-ray photoelectron spectroscopy (XPS) can be used to determine the oxidation states of metals present in the MOF. Finally, nuclear magnetic resonance (NMR) is also a common method used to analyse MOFs.

Due to enormous number of ways in which the wide variety of SBUs and organic linkers can combine to form MOFs, over the last few years, over 20,000 different MOFs have been reported. Their chemical and thermal stability, ultrahigh porosity, large internal surface areas and other physical and chemical properties make them suitable for a variety of uses. MOFs have found applications ranging from use in gas storage, gas separation and supercapacitors to use in catalysis, biomedical imaging and drug delivery [36, 37, 34].

MOFs are promising materials for heterogenous catalysis due to their physical and chemical properties. The high density of homogeneously distributed active sites in these crystalline materials, along with their ultrahigh porosity, large internal surface areas, overall chemical and physical stability, and most importantly, their tunable nature makes them ideal materials for efficient catalysts. For example, their architecture can be altered by using suitable SBUs and organic ligands to produce MOFs with desired geometrical structures. It

is also possible to change the pore sizes of MOFs while maintaining the same architecture by using longer or shorter ligands (isoreticular synthesis). All this is extremely useful for controlling which molecules can enter and leave the pores of the MOF. It is also possible to change the chemical properties of the pores in an already formed MOF by PSM. This can be used to dangle certain functional groups that behave as active sites within the pores of MOFs [36, 37, 29, 38]. MOFs can also be used directly as catalysts if they have been activated (by heating in vacuum to remove coordinated water molecules from the SBUs) to create open metal sites that behave as Lewis acid catalysts. Due to their permanent porosity and tunable pore sizes, MOFs are ideal support materials for active species such as MNPs. MOFs can be used to create hybrid catalysts such as MNPs@MOF materials and MNPs/MOF materials. Both these materials behave as excellent catalysts due to synergistic effects between the MOF and the MNPs. In these hybrid materials, MNPs act as the active sites and the MOFs help stabilize the MNPs. This is the simplest form of synergy that is present between MNPs and MOFs in these hybrid structures, and it is the reason for the improved activity (as compared to the activity of either of the individual components). Although it depends on the exact reaction and catalyst, in general, MNPs@MOF materials are preferred over MNPs/MOF as they often show better catalytic activity. The confinement of active species within the pores of MOFs has numerous advantages over using the active species directly. For example, in the case of MNPs@MOF materials the MNPs do not get leached and they are not allowed to clump together. The pores can also act as molecular sieves and allow only desired substrate molecules to enter the MOF and reach the active sites. By controlling pore size, size-selective catalysts which act only on substrates of a specific size can be created by excluding large substrates from the pores. Furthermore, the pore shapes can be designed to force substrates to enter the active sites containing pores with a particular orientation. This can be used to create stereoselective catalysts. All this can greatly help in preventing unwanted side-reactions, thereby increasing the selectivity of the catalysts. Confining active species with the pores of MOFs can also be used to heterogenize well-known homogeneous catalysts such as porphyrins or enzymes. These hybrid materials carry the advantages of both heterogenous and homogenous catalysts as high activity can be maintained while still being able to separate the active species from the products. In short, MOFs emerge as novel materials with a number of properties that make them potential candidates for highly effective catalysts [39, 40, 41, 42, 43].

Chapter 2

Motivation

2.1 Photocatalysis and Cerium

It was discussed in the previous chapter that MOFs are materials that can potentially be engineered to behave as effective catalysts for specific chemical reactions. In our case, the focus was to find a suitable MOF that can dehydrogenate AB in the non-aqueous medium in an efficient manner for use in on-board hydrogen storage systems. Here, using MOF based photocatalysts was an option that looked interesting as this allows the rate at which AB is dehydrogenated to be controlled precisely (for example by varying the light intensity). This is extremely useful on-board as it allows the supply of hydrogen to the fuel cell to be controlled as per the energy requirements. Also, it allows for high rates of reaction to be achieved at low temperatures by using light to enhance the catalytic activity rather than heat. This is an important advantage as it is neither safe nor practical to maintain high temperatures on-board. For these reasons, we tried to investigate MOFs which may behave as photocatalysts.

We decided to use cerium based MOFs with the UiO-66 architecture for our reactions as these MOFs are known to be photocatalytically active [31]. The UiO-66 architecture is highly robust and stable. It demonstrates excellent chemical, thermal, and mechanical stability and it was chosen for these reasons. Cerium was chosen as the primary metal due to its unique nature. Cerium is one of the few lanthanides that has 2 stable oxidation states (3+ and 4+). Typically, in a MOF, the photocatalytic activity of a material depends on the lifetime of the excited states. Therefore, for photocatalysis to occur, it should be possible for charge carriers to stay separate without recombining too quickly. In a MOF, to prolong the lifetime of the excited states, electrons that have been photoexcited in the ligand should ideally be able to move into an unoccupied orbital in the metal ion. This ligand-to-metal charge transfer (LMCT) helps create a separation of charge carriers that is necessary for photocatalysis. Cerium based MOFs with the UiO-66 architecture contain Ce^{4+} ions with empty, low-lying 4f orbitals that can be filled by photoexcited electrons from ligands to form Ce^{3+}

ions [33, 44]. This explains why cerium based MOFs with the UiO-66 architecture that contain Ce^{4+} ions in the SBUs are photocatalytic. It is for these reasons that we chose these MOFs for our investigation.

2.2 Platinum Nanoparticles

We decided to embed platinum NPs inside the pores of the cerium MOFs with the UiO-66 architecture for multiple reasons. It is well-known that platinum NPs are highly active catalysts for the dehydrogenation of AB both in the aqueous medium and the non-aqueous medium [25, 23]. Although it depends on the reaction and the material used, as highlighted in the previous chapter, many studies have revealed that, more often than not, MNPs@MOF materials exhibit catalytic properties that are superior to MNPs/MOF materials, and MOFs or MNPs alone [43]. By using MOFs as a support framework for the NPs, we hoped for synergistic effects between the two to yield highly efficient catalysts for the dehydrogenation of AB in a non-aqueous medium. As explained previously, the UiO-66 framework was selected mainly due to its robustness and overall stability [31]. Since we were also interested in a photocatalytic system, cerium was chosen as the primary metal [33, 44]. This is why we chose cerium MOFs with the UiO-66 architecture for our investigation.

Cerium MOFs with the UiO-66 architecture are known to have photocatalytic properties [33]. It has been demonstrated that MNPs which are embedded within photocatalytic MOFs tend to accept photo-excited electrons [43]. It is thought that embedding MNPs can help enhance the photocatalytic properties of the MOFs. This is because MNPs may behave as electron reservoirs and help to improve the separation and lifetime of charge carriers that have been generated by photoactivation. In certain cases, it has been shown that, in the case of photocatalytic MOFs, MNPs@MOF materials demonstrate higher catalytic activity than MNPs/MOF materials or the MOF alone [43]. For all these reasons we chose to experiment with embedding platinum nanoparticles within cerium based MOFs with the UiO-66 architechture to create efficient catalysts for the photocatalytic dehydrogenation of AB.

2.3 Amine Functionalization

Apart from the experiments with the UiO-66 cerium MOF and the Pt@UiO-66 cerium MOF, we also decided to conduct experiments with the NH_2-UiO-66 cerium MOF and Pt@NH_2-UiO-66 cerium MOF. This was inspired by studies that employed amine-functionalised zirconium based UiO-66 MOFs for photocatalytic reactions. In the reactions, the Pt@NH_2-UiO-66 zirconium MOF, the Pd@NH_2-UiO-66 zirconium MOF and the NH_2-UiO-66 zirconium MOF were shown to be effective photocatalysts [43, 45, 46, 47]. To try and understand the effects of the amine group on the photocatalytic activity, we conducted experiments using NH_2-UiO-66 Cerium MOF and Pt@NH_2-UiO-66 Cerium MOF catalysts for the dehydrogenation of AB.

Chapter 3

Experimental Details

3.1 Apparatus Used

Standard equipment available in most chemistry research laboratories was used for the investigation. PXRD patterns were recorded on a D2 Phaser Bruker Powder X-ray Diffractometer using Cu-Kα radiation with a wavelength of 1.5418 Å. An annular visible light photoreactor with a 500 W tungsten metal halide lamp was used during the photocatalytic reactions. Cold water was circulated around the lamp using a jacket to prevent overheating. To measure the volume of hydrogen released when AB was dehydrogenated, a unique gas displacement system (shown in the figure on the next page) was used.

This setup has a number of advantages over conventional gas displacement systems which are used to measure the volume of gas evolved during a reaction. The bubbling tube is connected to a Schlenk tube which contains the reaction mixture (AB and the catalyst in a solvent). Once the reaction begins, hydrogen is released. Hydrogen moves from the Schlenk tube into the bubbling tube and it gets bubbled through the water which is present. This makes it easy to verify that some hydrogen is in fact being evolved. The hydrogen then moves up through the rubber pipe and enters the graduated tube which is filled with water. As it builds up here, it pushes down on the water and causes the water level in the reservoir to rise. As the reaction takes place, the level of water in the graduated tube falls and the level of water in the reservoir rises. This allows us to record the volume of hydrogen released at regular time intervals by using the markings on the graduated tube. The biggest advantage with this setup is the possibility to correct the volume for pressure differences, thus making it possible to calculate the number of moles of hydrogen released. The following example illustrates this. At the end of the reaction, let us assume that the volume of hydrogen released as seen on the graduated tube is V_f (we assume that initially the water level was at the zero level). Since the water in the reservoir is at a higher level, it is clear that the pressure of the hydrogen gas is greater than that of atmospheric pressure. But since we do not know what the pressure is, it is

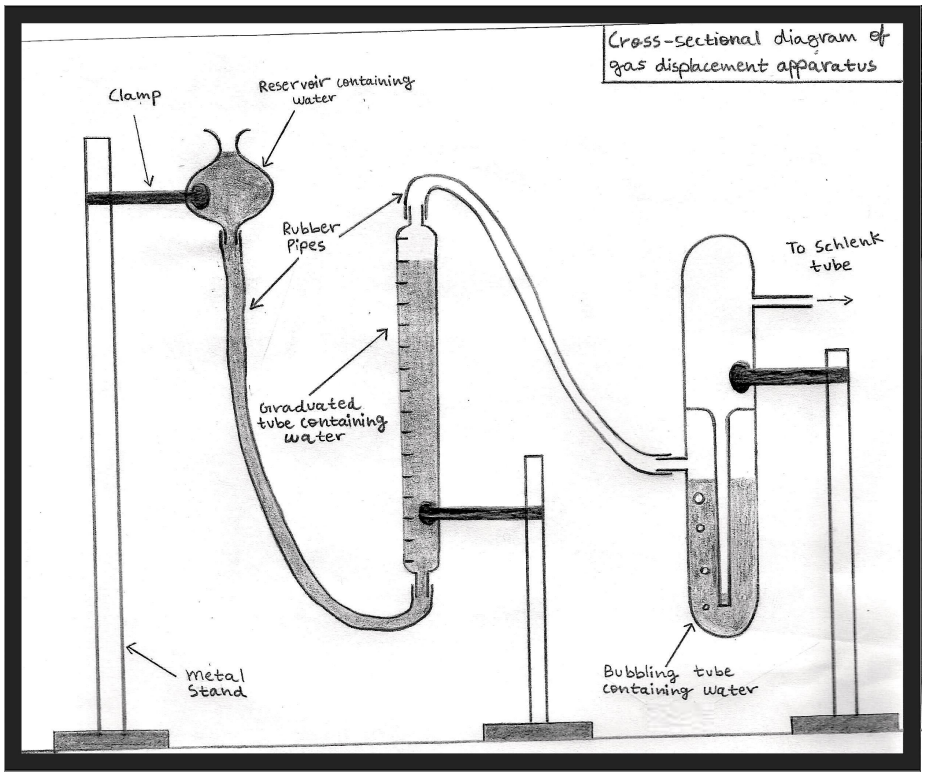

Figure 3.1: Cross-sectional diagram of the gas displacement apparatus.

difficult for us to judge how much hydrogen (in terms of moles) has actually been released. However, with this setup, the reservoir can be lowered on the metal stand until the water level in the reservoir matches the water level in the graduated tube. Then, since the water levels are the same, the pressure of the hydrogen gas in the graduated tube must be equal to atmospheric pressure. Now, we can record the final corrected volume of hydrogen $\mathrm{V_{fc}}$ using the marks on the graduated tube. The ideal gas equation $PV/RT = n$ can be used to calculate the number of moles of hydrogen which have been released (because P = 1 atmosphere and T = room temperature). Furthermore, if it any earlier time, the volume of hydrogen in the graduated tube was $\mathrm{V_t}$ then the corrected volume at that time $\mathrm{V_{tc}}$ can be given by the $V_{\mathrm{tc}} = V_{\mathrm{t}} \times (V_{\mathrm{fc}}/V_{\mathrm{f}})$. Of course, all this is based on certain conditions that must be met. Initially, at the start of the experiment, the following must be true: 1) the water level in the graduated tube is at the zero level; 2) the water level in the reservoir is approximately matches the water level in the graduated tube (else there would be a large zero error); 3) changes in temperature are negligible; 4) all gases behave ideally. This calculation also assumes that the pressure of the hydrogen gas is a constant

through the experiment. In short, this entire setup is very useful. The diagram below shows a Schlenk tube.

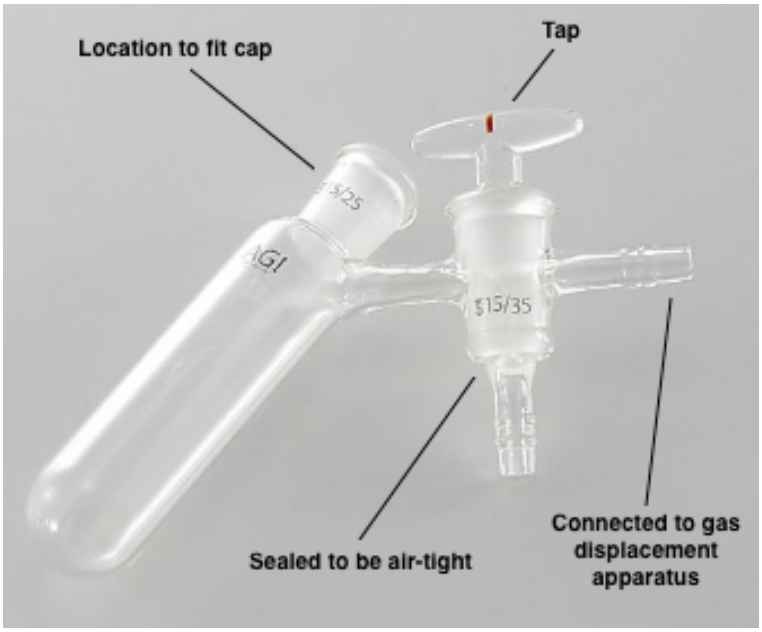

Figure 3.2: Diagram of a Schlenk tube. Image adapted from reference [48].

3.2 Synthesis Methods

Ammonia Borane: A typical salt metathesis procedure as reported in literature was used [21]. Equal moles of sodium borohydride ($NaBH_4$, 0.945 g, 0.025 M) and ammonium sulphate (NH_4SO_4, 3.303 g, 0.025 M) were separately ground to a fine powder using a mortar and pestle. Both powders were then mixed and added to a 250 ml round bottomed flask along with a magnetic bead and dry tetrahydrofuran (THF, 150 ml). The flask was then placed in an oil bath under stirring at 40 °C and the top of the flask was connected to a leigbig condenser with water at 5 °C circulating through it. The reaction was allowed to occur for 2 hours. The reaction mixture was then filtered with filter paper and the filtrate was collected (AB dissolved in THF). The residue (Na_2SO_4) was discarded. A rotary evaporator was used to collect the AB which was dissolved in the filtrate. The collected AB was dried under vacuum for 30 minutes. A powdery white solid was obtained.

UiO-66 Cerium MOF: A standard synthesis procedure as reported in literature was used with minor modifications [31, 49]. Terephthalic acid (H_2BDC, 708 mg) and N,N-dimethylformamide (DMF, 24 ml) were measured and added to a 100 ml screw capped jar. The mixture was sonicated for 20 minutes to ensure that the solid terephthalic acid dissolved completely. Ceric ammonium nitrate ($(NH_4)_2Ce(NO_3)_6$, 7.305 g) and distilled water were used to prepare an aqueous solution (0.533 M) in a 25 ml volumetric flask. 8 ml of the Ceric ammonium nitrate solution was then added (along with a magnetic bead) to the 100 ml screw capped jar containing the other reactants. The cap was shut tightly, and the jar was placed in an oil bath under stirring at 100 °C for 15 minutes. A color change from orange to cream/white was observed. The newly formed material was washed 3 times with 20 ml of N,N-dimethylformamide, and then washed another 3 times with 20 ml of acetone using a centrifuge. The washed material was then dried under vacuum for a period of 1 hour. A cream/white collared powder was obtained.

NH_2-UiO-66 Cerium MOF: A self designed solvent-assisted linker exchange (SALE) synthesis procedure was used. 2-Aminoterephthalic acid (NH_2BDC, 1 g) N,N-dimethylformamide (DMF, 50 ml) and distilled water (15 ml) were added to a 100 ml round bottomed flask. The mixture was sonicated for 1 hour to ensure that the solid 2-aminoterephthalic acid dissolved completely. A previously prepared sample of UiO-66 cerium MOF (500 mg) was added to the flask and the mixture was sonicated for 1 hour. A magnetic bead was added to the flask and it was kept under stirring in an oil bath 70 °C for 10 hours without a cap (open top synthesis). A color change from cream/white to orange-brown was observed. The newly formed material was washed 3 times with 20 ml of N,N-dimethylformamide, and then washed another 3 times with 20 ml of acetone using a centrifuge. The washed material was then dried under vacuum for a period of 1 hour. An orange-brown powder was obtained.

Embedding platinum nanoparticles into MOFs: A standard procedure as reported in literature was used after some significant modifications [50]. A 1% by weight Pt@MOF material was prepared. The same procedure was followed for both the MOFs (UiO-66 cerium MOF and NH_2-UiO-66 cerium MOF). 500 mg of the MOF along with 30 ml of distilled water were added to a 100 ml screw cap flask. The mixture was sonicated for 1 hour to disperse the MOF thoroughly. Chloroplatinic acid hexahydrate ($H_2PtCl_6.6H_2O$, 13.275 mg) was dissolved in 7.5 ml of distilled water in a vial. A magnetic bead was added to the flask and the solution in the vial was added dropwise into the flask under stirring. The cap was shut and the mixture was allowed to stir for 20 hours at room temperature. The mixture was then washed 3 times with 30 ml of distilled water using a centrifuge. The solid material was then transferred to a 100 ml screw capped flask (from the centrifuge tube) and dispersed in 10 ml of distilled water for 20 minutes by sonication. Sodium borohydride ($NaBH_4$, 10 mg) was dissolved in 5 ml of distilled water in a vial. A magnetic bead was added to the flask and the flask was then cooled in an ice bath. The sodium

borohydride solution was added to the flask dropwise under stirring (this was done to reduce the Pt^{2+} ions inside the pores of the MOF to Pt metal). The material was observed to become darker in color. The cap was shut and the mixture was allowed to stir for 1 hour. After this, the material was washed 3 times with 30 ml of distilled water and then 3 times with 20 ml of acetone using a centrifuge. Finally, the material was dried under vacuum for 1 hour. The Pt@UiO-66 Cerium MOF material was grey in color while the Pt@NH_2-UiO-66 Cerium MOF material was observed to be dark brown in color.

3.3 Experimental Procedures

A total of 26 reactions were conducted, out of these, 13 were done in the absence of light while 13 were done in the presence of light (in the photoreactor). For each of the 4 different catalysts used, the reaction was repeated 3 times in the absence of light and 3 times in the presence of light. 2 control experiments without any catalyst were also conducted (1 in the absence of light and 1 in the presence of light). The 4 different catalysts which were tried were:

1. UiO-66 Cerium MOF
2. Pt@UiO-66 Cerium MOF
3. NH_2UiO-66 Cerium MOF
4. Pt@NH_2-UiO-66 Cerium MOF

For each of the reactions, the following sequence of steps were followed:

1. 20 mg of the catalyst was weighed into a Schlenk tube
2. A small magnetic bead (rice pellet) was added to the Schlenk tube
3. The Schlenk tube was firmly connected to the gas displacement apparatus
4. The tap of the Schlenk tube was shut and the gas displacement apparatus was adjusted such that the level of water in the graduating tube was at the zero mark. The height of the reservoir was adjusted so that the water level in the reservoir matched the water level in the graduating tube.
5. 31 mg (1 mmol) of AB was dissolved in 1 ml of the solvent 1,4 dioxane in a vial
6. The solution of AB was drawn into a plastic syringe and injected rapidly into the Schlenk tube after opening the cap
7. The cap of the Schlenk tube was shut immediately, the magnetic stirrer was turned on and the tap was opened

8. For reactions in the absence of light, the reactions were conducted in a dimly lit room while the Schlenk tube was covered with aluminium foil. For reactions in the presence of light, the Schlenk tube was placed in the photoreactor at a fixed distance from the lamp, and the lamp was turned on immediately after adding the AB

9. the volume of hydrogen released was recorded every minute for 30 minutes

10. The final corrected volume was recorded after lowering the water level in the reservoir to the appropriate level.

Before each of reactions, to ensure that there were no leaks, all the pipes in the gas displacement apparatus were connected firmly and grease was applied to the tap and the cap of the Schlenk tube. During all the reactions, the temperature was maintained at 40 °C and the reaction was conducted for a period of 30 minutes. The volume of hydrogen evolved during every minute of the reaction was recorded. All reactions were conducted under stirring.

The final corrected volume (V_{fc}), the final volume (V_f), and the values of the volume at every minute (V_t values) were used to calculate the corrected values of the volume at every minute (V_{tc} values). These values were later used to plot graphs (corrected volume of hydrogen (Y-axis) against time (X-axis)) which were used for the purpose of analysis. For each catalyst, the mean final corrected volume of hydrogen was calculated (using the values from the repeat reactions) for both set of reactions (those in the presence of light and those in the absence of light). This data was used to a plot bar chart and it was also used for statistical analysis. All this information is presented in the next chapter.

Chapter 4

Results and Analysis

4.1 Characterization

The MOFs were characterized using PXRD. The image below shows the diffraction patterns for the MOFs. The simulated pattern was constructed using data from the Cambridge Crystallographic Data Centre (CCDC).

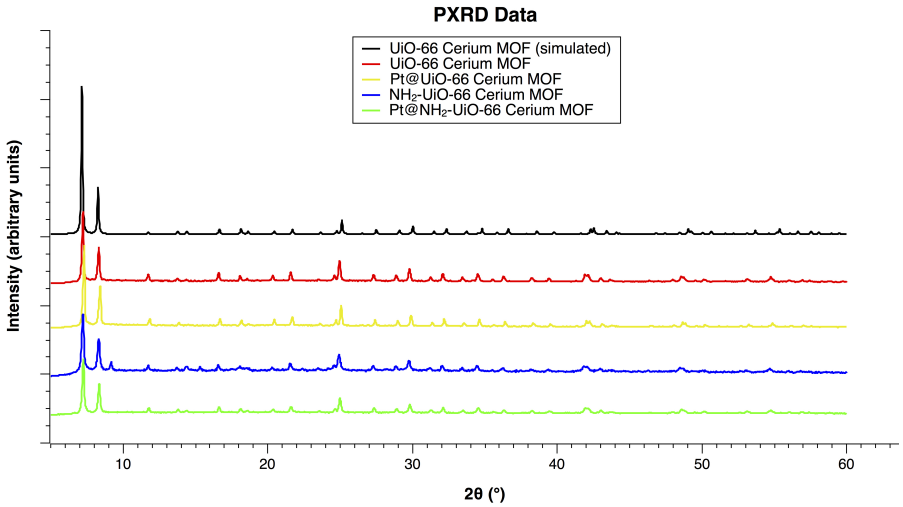

Figure 4.1: PXRD patterns of the MOFs. The graphs have been offset along the vertical axis for clarity.

It can be seen that the peaks in the diffraction patterns of all the synthesized materials match closely with those in the simulated pattern. This suggests that all the materials have the same, regular, crystalline three-dimensional UiO-66 architecture. Thus, we can be sure that the process of synthesis has been suc-

cessful and that all the MOFs have formed. It should be mentioned that the diffraction pattern for the NH_2-UiO-66 cerium MOF contains an extra peak (approximately when $2\theta \approx 9$) and displays more noise than the diffraction patterns of other materials. The reason for this is not clear, but since the pattern strongly resembles the simulated pattern, it can be reasonably assumed that the MOF has formed. The formed MOFs were then used in the reactions to investigate their photocatalytic properties.

4.2 Experimental Data

Control experiments which were conducted without any catalyst showed no release of hydrogen from AB (both in the presence and absence of light). This allowed us to reasonably conclude that if there is any release of hydrogen from AB in the other reactions, then it must be due to the presence of the catalyst.

As mentioned previously, reactions were conducted 3 times with each of the 4 different MOF catalysts in the presence of light, and 3 times in its absence. The graphs given below show the hydrogen evolution data from the reactions. In each case, the corrected volume of hydrogen released (Y-axis) is plotted against time (X-axis). These graphs were used to investigate the catalytic activity of the different MOFs and compare them with each other.

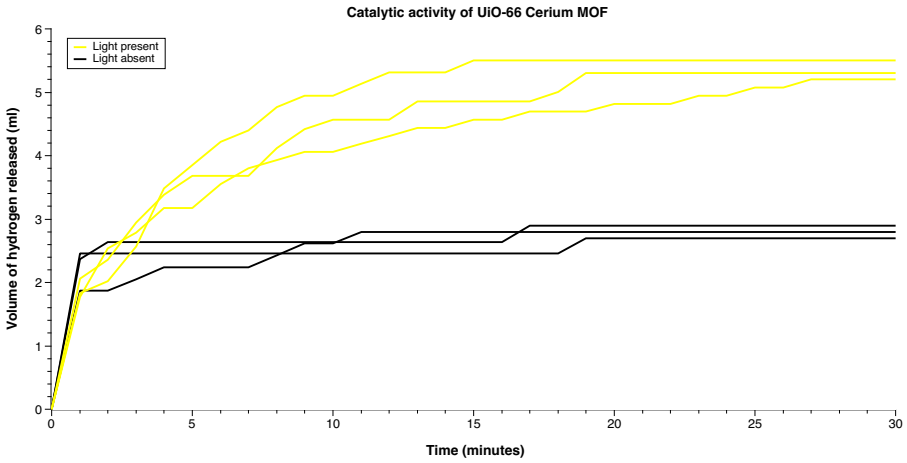

Figure 4.2: Catalytic activity of UiO-66 cerium MOF.

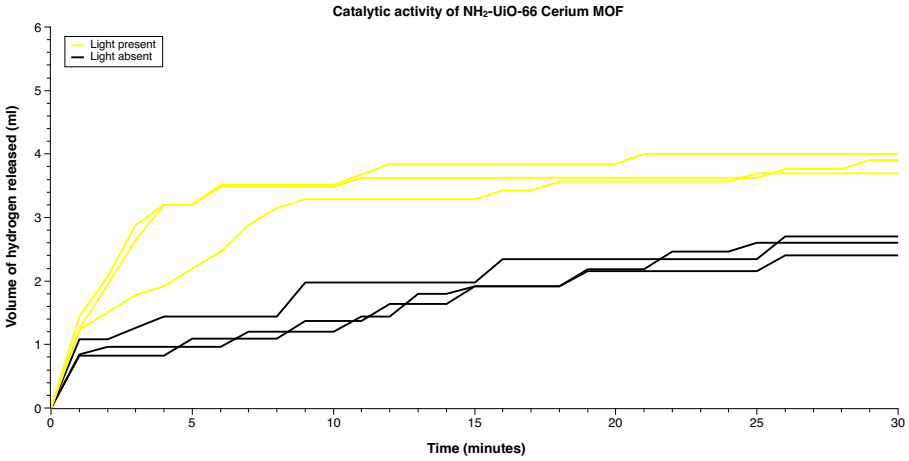

Figure 4.3: Catalytic activity of NH_2-UiO-66 cerium MOF.

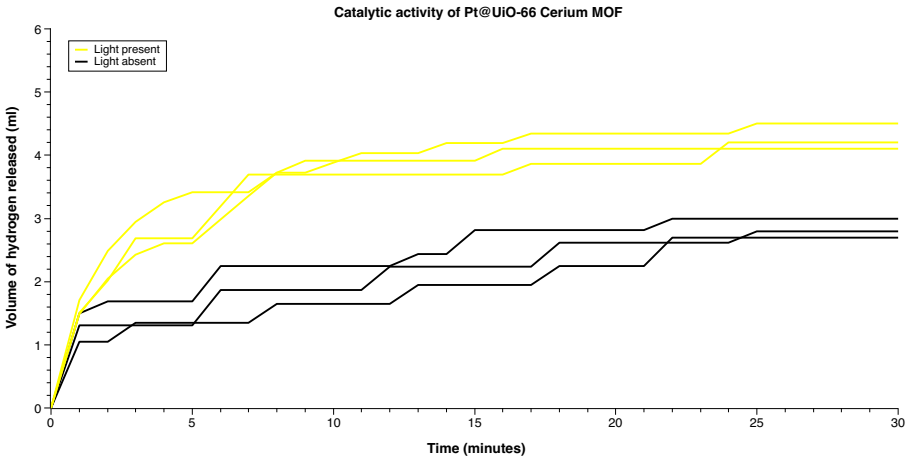

Figure 4.4: Catalytic activity of Pt@UiO-66 cerium MOF.

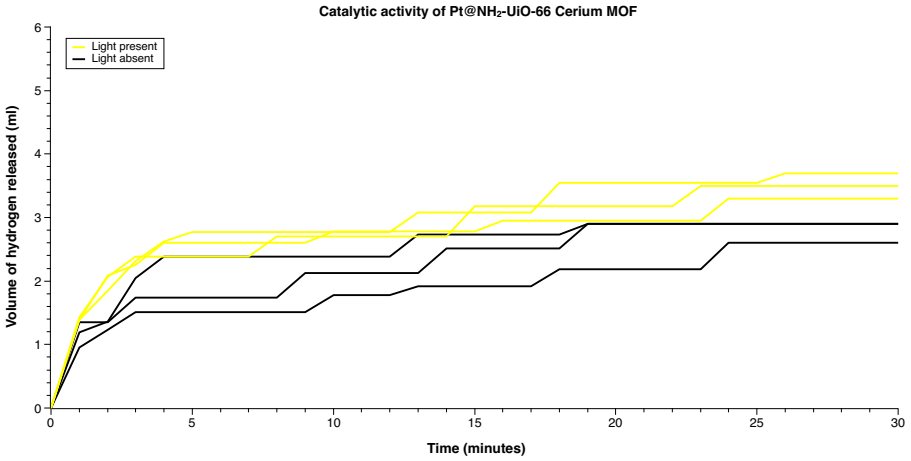

Figure 4.5: Catalytic activity of Pt@NH_2-UiO-66 cerium MOF.

From the graphs it can be inferred that the catalysts behave in a fairly consistent and reliable manner. This is because the corrected volume of hydrogen released in 30 minutes is approximately the same when a given experiment is repeated. Furthermore, for all the catalysts, the activity in the presence of light seems to be higher than the activity in the absence of light. For a given catalyst, since the temperature and other conditions are kept constant, this strongly suggests that photocatalysis is indeed taking place. The effect of light on catalytic activity seems to be most prominent in the UiO-66 cerium MOF, and least prominent in the Pt@NH_2-UiO-66 cerium MOF. With the other two, the effect of light on the catalytic activity seems to be slightly more in the case of the Pt@UiO-66 cerium MOF as compared to the NH_2-UiO-66 cerium MOF. Looking directly at the catalytic activity in the absence of light, all the catalysts seem to behave in a very similar manner. In the presence of light things seem to work quite differently. The UiO-66 Cerium MOF seems to perform the best, followed by the Pt@UiO-66 Cerium MOF. The Pt@NH_2-UiO-66 Cerium MOF seems to be the worst performing catalyst, and the NH_2-UiO-66 Cerium MOF is only slightly better. All this seems to suggest that introducing amine groups and platinum nanoparticles have no effect at all in the absence of light, and lower the catalytic activity in the presence of light.

As one would expect, the rate of reaction (given by the gradient of the graphs) falls with time due to the decreasing concentration of AB. Ideally we should have obtained smooth curves for the graphs, but here, we have jagged lines. This is mainly due to the apparatus used and methods to improve the experimental measurements will be discussed in a separate section. But, since the corrected volume at the end of 30 minutes is what is most important to us, this is not a major problem.

To conclude, all that we have noticed could be due to random chance. We

do not know if the differences in catalytic activity under different conditions are significant or not. To quantify this and make conclusions more confidently, statistical tests are required. In particular, we will use the Student's t-test. This will be used to distinguish and compare the effects of introducing amine groups, platinum nanoparticles, and light on the catalytic activity of the MOFs in a clear and concise manner.

4.3 Analysis and Discussion

We will first look at a bar chart comparing the mean catalytic activity of the different MOFs in the presence and absence of light. Here, both in the presence of and absence of light, the mean final corrected volume of hydrogen after 30 minutes was calculated for each catalyst using values of the final corrected volume from the 3 repeat experiments. Error bars were plotted on the chart using the standard error of the mean which was itself calculated by using the standard deviation. The image below shows the bar chart.

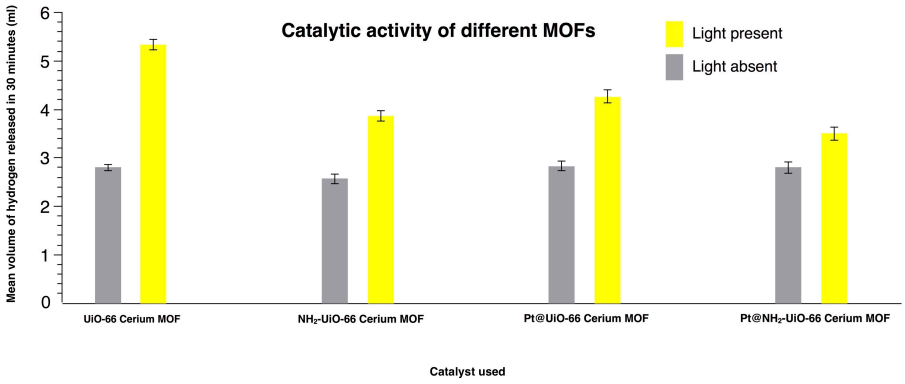

Figure 4.6: Catalytic activity of MOFs.

This graph neatly summarizes what we observed in the previous section. If we compare the activity of each catalyst in the presence and absence of light, we can see that the activity is higher in the presence of light. It appears that this difference is significant as the error bars do not overlap and are far from each other. This makes it likely that the t-test will indicate a significant difference. Similarly, if we compare the activity of the catalysts in the absence of light, we can see that they are roughly similar as the bars are of similar height and the error bars overlap or are very close to each other. This suggests that the t-test will indicate no significant difference. In the presence of light, what we noticed earlier is depicted clearly on the chart.

We can now proceed to quantify the comparisons and make concrete conclu-

sions from our data set. The Student's t-test was chosen for multiple reasons, but mainly because it facilitates the comparison of the means of two continuous sets of quantitative data to check whether or not they are significantly different. We used the two-tailed sample-equal t-test. There are certain criteria that must be satisfied for the effective use of statistical tests [51]. For the Student's t-test, both data sets must be continuous, quantitative data. This is satisfied in our case. Each data set must have a normal distribution, and it is reasonable to assume that this is so in our case as the data is both continuous and quantitative. Furthermore, the standard deviations of the separate data sets must be similar in size. This is also satisfied in our case. Finally, each data set must ideally have between 10 and 30 individual readings. Here, our data sets do not meet the required criterion as each data set has only 3 individual readings. Even so, we decided to employ the t-test as these rules are not set in stone. Since the t-test makes adjustments by taking into account the degree of freedom, it is reasonable to suppose that it can be used fairly effectively even in our case. Ideally, the entire investigation would have been more credible if each experiment was conducted 10 times or more. But cost plays a role here. The chemicals used to synthesise MOFs are very expensive (especially the platinum precursor) and this makes it difficult to repeat experiments many times.

As is standard, a probability of 0.05 (5%) was taken to be the critical probability. The null hypothesis which states that there is no significant difference between the means of the two given data sets was used as a starting point. According to this, we may say that a t-value which corresponds to a probability of less than 0.05 is possible only if there is a significant difference between the means of the two data sets, and that the difference is not simply an effect of random chance. The data tables on the next page show the results of the statistical analysis. Three tables have been constructed to try and treat the effect of light, amine groups, and platinum NPs on the catalytic activity of the MOFs separately.

The topmost table shows the effect of light on the catalytic activity of each of the 4 MOFs. This table clearly shows what we noticed earlier in our analysis using the graphs and the bar chart. Since the t-values for each of the MOFs correspond to a probability of less than 0.05, it means that the catalytic activity is significantly higher in the presence of light. This confirms that there is indeed photocatalysis taking place. The data from this table also shows us that the UiO-66 cerium MOF is the primary material and that platinum NPs and amine groups are themselves not necessary for photocatalysis.

EFFECT OF LIGHT ON CATALYTIC ACTIVITY IN DIFFERENT MOFS

Catalyst	UiO-66 Cerium MOF		NH_2-UiO-66 Cerium MOF		Pt@UiO-66 Cerium MOF		Pt@NH_2-UiO-66 Cerium MOF	
Light	Absent	Present	Absent	Present	Absent	Present	Absent	Present
Mean volume of hydrogen released in 30 minutes (ml)	2.80	5.33	2.57	3.87	2.83	4.27	2.80	3.50
Student's *t*-test probability value	0.000018		0.00024		0.00033		0.0051	
Significant difference	YES		YES		YES		YES	

EFFECT OF EMBEDDED PLATINUM NANOPARTICLES ON CATALYTIC ACTIVITY IN DIFFERENT MOFS

Catalyst	UiO-66 Cerium MOF				NH_2-UiO-66 Cerium MOF			
Light	Absent		Present		Absent		Present	
Embedded platinum nanoparticles	Absent	Present	Absent	Present	Absent	Present	Absent	Present
Mean volume of hydrogen released in 30 minutes (ml)	2.80	2.83	5.33	4.27	2.57	2.80	3.87	3.50
Student's *t*-test probability value	0.77		0.0020		0.16		0.065	
Significant difference	NO		YES		NO		NO	

EFFECT OF AMINE GROUPS ON CATALYTIC ACTIVITY IN DIFFERENT MOFS

Catalyst	UiO-66 Cerium MOF				Pt@UiO-66 Cerium MOF			
Light	Absent		Present		Absent		Present	
Amine group	Absent	Present	Absent	Present	Absent	Present	Absent	Present
Mean volume of hydrogen released in 30 minutes (ml)	2.80	2.57	5.33	3.87	2.83	2.80	4.27	3.50
Student's *t*-test probability value	0.091		0.00030		0.81		0.010	
Significant difference	NO		YES		NO		YES	

Figure 4.7: Data tables and statistical analysis.

The central table shows the effect of embedding platinum NPs on the catalytic activity of each of the 2 MOFs. If we look at the UiO-66 cerium MOF, we can see that there is no significant change in the catalytic activity when there is no light. In the presence of light, there is a significant decrease in catalytic activity. This is the opposite of what we expected and desired. Since it is already known that platinum NPs catalyse the dehydrogenation of AB in the non-aqueous medium, and that the UiO-66 cerium MOF is a photocatalyst, we expected there to be a higher activity (both in the presence and absence of light). We had hoped that in the presence of light, the platinum NPs would enhance the photocatalytic properties of the MOF via synergistic effects. The reason for the significant decrease in the photocatalytic activity of the UiO-66 cerium MOF due to the introduction of platinum NPs is not clear. It is possible that the platinum nanoparticles are somehow interacting with the cerium ions in the MOF and modifying their electronic properties in a way such that they are not as photoactive anymore. This inhibitory effect could be the cause for the decrease in activity. If we move to the NH_2-UiO-66 cerium MOF, we no-

tice something slightly different. In the absence of light, there is no significant difference just like in the case of the UiO-66 cerium MOF. In the presence of light, there is a decrease just like in the case of the UiO-66 cerium MOF, but it is not significant according to the t-test. Without further experimentation, this prevents us from generalizing that the introduction of platinum nanoparticles into the MOFs reduces their photocatalytic activities signficantly, but it may be possible that this is true.

The bottom-most table shows the effect of the amine group on the catalytic activity in different MOFs. Looking at the UiO-66 cerium MOF, we see that in the absence of light there is no significant decrease in the activity. In the presence of light, we notice that there is in fact a significant decrease in the activity. The same pattern is observed in the case of the Pt@UiO-66 cerium MOF. With this we can reasonably conclude that the introduction of the amine group reduces the photocatalytic activity of the MOFs. It is unclear as to why the activity decreased with the introduction of the amine groups, but it is possible that it is because of their basic nature. It is known that AB is dehydrogenated more readily by acidic catalysts (although this is mainly in the aqueous medium, it is also true in the non-aqueous medium). Since the UiO-66 cerium MOF is known to be acidic in nature, the introduction of amine groups may be reducing the overall acidity of the material, thus reducing its photocatalytic activity [52].

Chapter 5

Conclusion, Possible Improvements and Future Work

5.1 Conclusion

The ultimate aim of our investigation was to find a highly active catalyst for the dehydrogenation of AB in the non-aqueous medium for use in on-board hydrogen storage systems. We focused on MOFs, as their unable nature along with some of their chemical and physical properties make them excellent candidates for catalysts. In particular, we looked at cerium based MOFs with the UiO-66 architecture due to their durability and their photocatalytic properties. Using light to control the rate of reaction is an attractive option as it is suitable for the low temperature environments in on-board hydrogen storage systems. We also studied possible synergistic effects by introducing platinum NPs and amine groups into the MOFs. Overall we discovered that the UiO-66 cerium MOF and its variants (NH_2-UiO-66 cerium MOF, Pt@UiO-66 cerium MOF and Pt@NH_2-UiO-66 cerium MOF) were all photoactive materials as their effectiveness in dehydrogenating AB increased significantly when they were exposed to visible light. Although we hoped that introducing platinum NPs would help increase the photocatalytic activity of the MOFs due to synergistic effects, this did not happen. We found that in the case of the UiO-66 cerium MOF, the photocatalytic activity fell significantly, and in the case of the NH_2-UiO-66 cerium MOF, there was no significant effect on the photocatalytic activity. We also expected that introducing amine groups into our MOFs would promote the photocatalytic activity of the MOFs via synergistic effects, but once gain, this did not happen. It was found that in both the UiO-66 cerium MOF and the Pt@UiO-66 cerium MOF, introducing amine groups caused the photocatalytic activity to drop significantly. It was found that the pure UiO-66 cerium MOF was the

best photocatalyst. Unfortunately, even in the case of the UiO-66 cerium MOF, the catalytic activity was much lower than what is actually required for use in on-board hydrogen storage systems. This means that using the catalyst is not practical. In this sense, our investigation was not very successful. But it surely opens up the possibility of new areas of research which could focus on improving the photocatalytic properties of cerium based MOFs with the UiO-66 architecture, thus making them potential candidates for industrial applications.

5.2 Possible Improvements

In our investigation, there were areas where experiments lacked the necessary rigour and attention to detail which would have helped make the results more reliable. This section will discuss areas where improvements could have been made.

Some useful modifications to the synthesis procedures which were used would have surely helped our overall investigation. There are two well known methods to embed metal nanoparticles into MOFs to make the metal@MOF materials. The method we used involves embedding metal ions into the pores of MOFs prior to reducing them with a reducing agent. The other option, which is known as the ship-in-a-bottle approach, involves growing the MOF around suspended metal NPs in a solution may have been a better option as it is more effective. For the synthesis of the NH_2-Uio-66 cerium MOF, we used a solvent-assisted linker-exchange (SALE) method. The issue with this is that it tends to form a mixed-linker MOF containing both the amine functionalized linker and the ordinary linker. It would have probably been better to synthesise the MOF directly by using 2-aminoterephthalic acid as the linker using the process reported in literature for the synthesis of the NH_2-UiO-66 zirconium MOF [53]. Since both the MOFs have the same UiO-66 architecture, it is likely that replacing the cerium precursor with the zirconium precursor will still lead to a successful synthesis. This method ensures that the entire MOF is made only from a single linker rather than a mixture, and it also makes the process more easily reproducible.

Our investigation would have also benefited enormously from more extensive characterization of synthesized materials. In the case of AB, although we used a well-known synthesis method, it would have been best to characterize the formed product using PXRD, FTIR spectroscopy, and ^{1}H and ^{11}B NMR to verify that AB had indeed formed [54]. The MOFs we synthesized were only characterized using PXRD. It would have been ideal if BET surface area and pore volume anaylsis was also done. This would help in the detection of any anomalous MOF structures, and it would also help to verify that metal NPs had indeed been embedded into MOFs. This is because embedding metals NPs will result in a lower pore volume and internal surface area. FTIR spectroscopy could have been used to quantify the number of amine groups in the MOFs that were synthesised via the SALE method. XPS could have been used to verify the oxidation state of metals in the formed materials (cerium and platinum). ICP-

OES could have been used to quantify the amount of platinum that actually entered the MOF and was embedded within it. Finally, bright field TEM would have been ideal to verify that metal nanoparticles were inside the MOF, and were not just scattered on the surface of the MOF.

In terms of the experimental apparatus, some useful modifications could have been made to the gas displacement system that was used to help make the results more accurate and precise. The main issue was that the volume of hydrogen released was low and so was the rate at which it was released. This made it difficult to take readings as there would only be very small changes for many minutes in a row which would be followed by a sudden increase. This is why the graphs shown earlier were made of jagged lines rather than being smooth curves. A possible solution to this problem would be to use a much narrower graduated tube with markings that are closer together (for example at every 0.05 ml). The other option would be to scale up the reaction by increasing the concentration of AB and increasing the mass of the catalyst that was used. This would cause more hydrogen to be released at faster rates, thus making it easy to make more accurate measurements with the same apparatus, but it would also result in a greater cost.

A few other things were missed out in our investigation. Ideally we should have should repeated each set of experiments at least 10 times to ensure the results were reliable and to also ensure that the data could be more suitable for the statistical analysis using the Students t-test. It would have also been good to conduct a set of control experiments using only suspended metal NPs as the catalyst.

5.3 Future Work

The entire investigation could have also been extended to include many other experiments. Experiments to measure the activity of the Pt/UiO-66 cerium MOF and Pt/NH_2-UiO-66 cerium MOF could have been conducted. This would help us see the effect of embedding MNPs within MOFs as compared to supporting MNPs on the surface of MOFs. The effect of other functional groups on the catalytic activity could have also been investigated (for example carboxylic acid groups or nitro groups). Other metals which are known to effectively dehydrogenate AB in the non aqueous-medium (such as palladium) could have also been tried. Experiments with other lanthanides (such as hafnium and zirconium) based MOFs with the UiO-66 architecture could have also been tried. Finally, a study focusing on varying the wavelength and intensity of the light used and seeing its effects on the photocatalytic activity of MOFs would have been an interesting venture. For example, the effect of high intensity laser light could have been studied.

Acknowledgments

I sincerely thank my mentor, Dr. Suresh Babu Kalidindi, for giving me the opportunity to work with him. He was open-minded enough to take me into his lab while I was still only a high school graduate and he introduced me to the exciting field of materials science. He was extremely patient, friendly and enthusiastic, and he always went out of his way to help me. I also thank Vasudeva Rao Bakuru and Marilyn Esclance DMello, PhD students of Dr. Suresh Babu Kalidindi, for their extensive help. They took time out of their busy schedule to help me operate instruments, teach me how to synthesize and characterize new materials, and with whatever else I needed. I am truly indebted to them. I also thank the other students, faculty and staff at the institute for all their help. Finally, I thank my parents and family for their tireless support.

Bibliography

[1] Stephen F Lincoln. Fossil fuels in the 21st century. *Ambio*, pages 621–627, 2005.

[2] Thomas R Karl and Kevin E Trenberth. Modern global climate change. *science*, 302(5651):1719–1723, 2003.

[3] Michael Le Page. Carbon dioxide levels will soar past the 410 ppm milestone in 2019. https://www.newscientist.com/article/2191881-carbon-dioxide-levels-will-soar-past-the-410-ppm-milestone-in-2019/, 2019.

[4] Rebecca Lindsey and LuAnn Dahlman. Climate change: Global temperature. https://www.climate.gov/news-features/understanding-climate/climate-change-global-temperature, 2018.

[5] Susan Solomon, Gian-Kasper Plattner, Reto Knutti, and Pierre Friedlingstein. Irreversible climate change due to carbon dioxide emissions. *Proceedings of the national academy of sciences*, 106(6):1704–1709, 2009.

[6] Glen P Peters, Robbie M Andrew, Tom Boden, Josep G Canadell, Philippe Ciais, Corinne Le Quéré, Gregg Marland, Michael R Raupach, and Charlie Wilson. The challenge to keep global warming below 2 c. *Nature Climate Change*, 3(1):4, 2012.

[7] Chris D Thomas, Alison Cameron, Rhys E Green, Michel Bakkenes, Linda J Beaumont, Yvonne C Collingham, Barend FN Erasmus, Marinez Ferreira De Siqueira, Alan Grainger, Lee Hannah, et al. Extinction risk from climate change. *Nature*, 427(6970):145, 2004.

[8] George W Crabtree, Mildred S Dresselhaus, and Michelle V Buchanan. The hydrogen economy. *Physics today*, 57(12):39–44, 2004.

[9] JO Abe, E Ajenifuja, and OM Popoola. Hydrogen energy, economy and storage: Review and recommendation. *International Journal of Hydrogen Energy*, 2019.

[10] IP Jain. Hydrogen the fuel for 21st century. *International journal of hydrogen energy*, 34(17):7368–7378, 2009.

[11] John A Turner. Sustainable hydrogen production. *Science*, 305(5686):972–974, 2004.

[12] Vasudeva Rao Bakuru, Marilyn Esclance DMello, and Suresh Babu Kalidindi. Metal-organic frameworks for hydrogen energy applications: Advances and challenges. *ChemPhysChem*, 20(10):1177–1215, 2019.

[13] Roger H Bezdek. The hydrogen economy and jobs of the future. *Renewable Energy and Environmental Sustainability*, 4:1, 2019.

[14] Xinghu Li and Xiaofeng Zhou. The properties of gasoline and effect of this properties on calculation of air-fuel ratio. Technical report, SAE Technical Paper, 2003.

[15] Tim Palucka and Brian J Ingram. Materials challenges in the hydrogen cycle. *MRS Bulletin*, 44(3):164–166, 2019.

[16] Bahman Zohuri. Hydrogen-powered fuel cell and hybrid automobiles of the near future. In *Hydrogen Energy*, pages 37–59. Springer, 2019.

[17] Sheldon G Shore and Robert W Parry. The crystalline compound ammonia-borane, 1 h3nbh3. *Journal of the American Chemical Society*, 77(22):6084–6085, 1955.

[18] Todd B Marder. Will we soon be fueling our automobiles with ammonia–borane? *Angewandte Chemie International Edition*, 46(43):8116–8118, 2007.

[19] Umit B Demirci. Ammonia borane, a material with exceptional properties for chemical hydrogen storage. *International Journal of hydrogen energy*, 42(15):9978–10013, 2017.

[20] Melanie C Denney, Vincent Pons, Travis J Hebden, D Michael Heinekey, and Karen I Goldberg. Efficient catalysis of ammonia borane dehydrogenation. *Journal of the American Chemical Society*, 128(37):12048–12049, 2006.

[21] P Veeraraghavan Ramachandran and Pravin D Gagare. Preparation of ammonia borane in high yield and purity, methanolysis, and regeneration. *Inorganic chemistry*, 46(19):7810–7817, 2007.

[22] Bo Peng and Jun Chen. Ammonia borane as an efficient and lightweight hydrogen storage medium. *Energy & Environmental Science*, 1(4):479–483, 2008.

[23] Roshan P Shrestha, Himashinie VK Diyabalanage, Troy A Semelsberger, Kevin C Ott, and Anthony K Burrell. Catalytic dehydrogenation of ammonia borane in non-aqueous medium. *International journal of hydrogen energy*, 34(6):2616–2621, 2009.

[24] Frances H Stephens, Vincent Pons, and R Tom Baker. Ammonia–borane: the hydrogen source par excellence? *Dalton Transactions*, (25):2613–2626, 2007.

[25] Manish Chandra and Qiang Xu. A high-performance hydrogen generation system: transition metal-catalyzed dissociation and hydrolysis of ammonia–borane. *Journal of Power Sources*, 156(2):190–194, 2006.

[26] Bahram Khan, Muhammad Bilal Khan Niazi, Zaib Jahan, Wasif Farooq, Salman Raza Naqvi, Majid Ali, Israr Ahmed, and Arshad Hussain. Effect of ultra-violet cross-linking on the properties of boric acid and glycerol co-plasticized thermoplastic starch films. *Food Packaging and Shelf Life*, 19:184–192, 2019.

[27] Thomas Gorman. Hexagonal boron nitride coating test on handgun ammo. http://www.boron-powder.com/hexagonal-boron-nitride-coating-test-on-handgun-ammo/, 2014.

[28] Wikipedia contributors. Sodium chloride, wikipedia, the free encyclopedia. https://en.wikipedia.org/w/index.php?title=Sodium_chloride&oldid=907079193, 2019. [Online; accessed 27-July-2019].

[29] Stuart R Batten, Neil R Champness, Xiao-Ming Chen, Javier Garcia-Martinez, Susumu Kitagawa, Lars Öhrström, Michael OKeeffe, Myunghyun Paik Suh, and Jan Reedijk. Terminology of metal–organic frameworks and coordination polymers (iupac recommendations 2013). *Pure and Applied Chemistry*, 85(8):1715–1724, 2013.

[30] Wikipedia contributors. Metal-organic frameworks, wikipedia, the free encyclopedia. https://en.wikipedia.org/w/index.php?title=Metal%E2%80%93organic_framework&oldid=908066420, 2019. [Online; accessed 27-July-2019].

[31] Martin Lammert, Michael T Wharmby, Simon Smolders, Bart Bueken, Alexandra Lieb, Kirill A Lomachenko, Dirk De Vos, and Norbert Stock. Cerium-based metal organic frameworks with uio-66 architecture: synthesis, properties and redox catalytic activity. *Chemical Communications*, 51(63):12578–12581, 2015.

[32] Kevin Hendrickx, Danny EP Vanpoucke, Karen Leus, Kurt Lejaeghere, Andy Van Yperen-De Deyne, Veronique Van Speybroeck, Pascal Van Der Voort, and Karen Hemelsoet. Understanding intrinsic light absorption properties of uio-66 frameworks: a combined theoretical and experimental study. *Inorganic chemistry*, 54(22):10701–10710, 2015.

[33] Xin-Ping Wu, Laura Gagliardi, and Donald G Truhlar. Cerium metal–organic framework for photocatalysis. *Journal of the American Chemical Society*, 140(25):7904–7912, 2018.

[34] Ashlee J Howarth, Aaron W Peters, Nicolaas A Vermeulen, Timothy C Wang, Joseph T Hupp, and Omar K Farha. Best practices for the synthesis, activation, and characterization of metal–organic frameworks. *Chemistry of Materials*, 29(1):26–39, 2016.

[35] Amarajothi Dhakshinamoorthy and Hermenegildo Garcia. Catalysis by metal nanoparticles embedded on metal–organic frameworks. *Chemical Society Reviews*, 41(15):5262–5284, 2012.

[36] Hiroyasu Furukawa, Kyle E Cordova, Michael OKeeffe, and Omar M Yaghi. The chemistry and applications of metal-organic frameworks. *Science*, 341(6149):1230444, 2013.

[37] Hong-Cai Zhou, Jeffrey R Long, and Omar M Yaghi. Introduction to metal–organic frameworks, 2012.

[38] Jesse LC Rowsell and Omar M Yaghi. Metal–organic frameworks: a new class of porous materials. *Microporous and mesoporous materials*, 73(1-2):3–14, 2004.

[39] Zhijie Chen, Junying Chen, and Yingwei Li. Metal–organic-framework-based catalysts for hydrogenation reactions. *Chinese Journal of Catalysis*, 38(7):1108–1126, 2017.

[40] JeongYong Lee, Omar K Farha, John Roberts, Karl A Scheidt, SonBinh T Nguyen, and Joseph T Hupp. Metal–organic framework materials as catalysts. *Chemical Society Reviews*, 38(5):1450–1459, 2009.

[41] Alexander U Czaja, Natalia Trukhan, and Ulrich Müller. Industrial applications of metal–organic frameworks. *Chemical Society Reviews*, 38(5):1284–1293, 2009.

[42] Marco Ranocchiari and Jeroen Anton van Bokhoven. Catalysis by metal–organic frameworks: fundamentals and opportunities. *Physical Chemistry Chemical Physics*, 13(14):6388–6396, 2011.

[43] Qihao Yang, Qiang Xu, and Hai-Long Jiang. Metal–organic frameworks meet metal nanoparticles: synergistic effect for enhanced catalysis. *Chemical society reviews*, 46(15):4774–4808, 2017.

[44] Kevin Hendrickx, Jonas J Joos, Arthur De Vos, Dirk Poelman, Philippe F Smet, Veronique Van Speybroeck, Pascal Van Der Voort, and Kurt Lejaeghere. Exploring lanthanide doping in uio-66: a combined experimental and computational study of the electronic structure. *Inorganic chemistry*, 57(9):5463–5474, 2018.

[45] Juan-Ding Xiao, Qichao Shang, Yujie Xiong, Qun Zhang, Yi Luo, Shu-Hong Yu, and Hai-Long Jiang. Boosting photocatalytic hydrogen production of a metal–organic framework decorated with platinum nanoparticles: The platinum location matters. *Angewandte Chemie International Edition*, 55(32):9389–9393, 2016.

[46] Dengrong Sun, Yanghe Fu, Wenjun Liu, Lin Ye, Dengke Wang, Lin Yang, Xianzhi Fu, and Zhaohui Li. Studies on photocatalytic co2 reduction over nh2-uio-66 (zr) and its derivatives: Towards a better understanding of photocatalysis on metal–organic frameworks. *Chemistry–A European Journal*, 19(42):14279–14285, 2013.

[47] Dengrong Sun and Zhaohui Li. Double-solvent method to pd nanoclusters encapsulated inside the cavity of nh2–uio-66 (zr) for efficient visible-light-promoted suzuki coupling reaction. *The Journal of Physical Chemistry C*, 120(35):19744–19750, 2016.

[48] https://www.sciket.com/product/group/11938, June 25th 2019.

[49] Chunlan Zhu, Tong Ding, Wanxian Gao, Kui Ma, Ye Tian, and Xingang Li. Cuo/ceo2 catalysts synthesized from ce-uio-66 metal-organic framework for preferential co oxidation. *International Journal of Hydrogen Energy*, 42(27):17457–17465, 2017.

[50] Zhiyong Guo, Chaoxian Xiao, Raghu V Maligal-Ganesh, Lin Zhou, Tian Wei Goh, Xinle Li, Daniel Tesfagaber, Andrew Thiel, and Wenyu Huang. Pt nanoclusters confined within metal–organic framework cavities for chemoselective cinnamaldehyde hydrogenation. *ACS Catalysis*, 4(5):1340–1348, 2014.

[51] Mary Jones, Richard Fosbery, Jennifer Gregory, and Dennis Taylor. *Cambridge International AS and A Level Biology Coursebook with CD-ROM*. Cambridge University Press, 2014.

[52] Vasudeva Rao Bakuru, Sathyapal R Churipard, Sanjeev P Maradur, and Suresh Babu Kalidindi. Exploring the brønsted acidity of uio-66 (zr, ce, hf) metal–organic frameworks for efficient solketal synthesis from glycerol acetalization. *Dalton Transactions*, 48(3):843–847, 2019.

[53] Hossein Molavi, Alireza Eskandari, Akbar Shojaei, and Seyyed Abbas Mousavi. Enhancing co2/n2 adsorption selectivity via post-synthetic modification of nh2-uio-66 (zr). *Microporous and Mesoporous Materials*, 257:193–201, 2018.

[54] Aysel Kantürk Figen, Mehmet Burçin Pişkin, Bilge Coşkuner, and Verda İmamoğlu. Synthesis, structural characterization, and hydrolysis of ammonia borane (nh3bh3) as a hydrogen storage carrier. *international journal of hydrogen energy*, 38(36):16215–16228, 2013.